Draft of February 9, 2018

The effect of wind stress anomalies and location in driving Pacific Subtropical cells and tropical climate

Giorgio Graffino*

ESFM Doctorate School, Università degli Studi di Trieste, Trieste, Italy, and Earth System Physics Section, International Centre for Theoretical Physics, Trieste, Italy

Riccardo Farneti

Earth System Physics Section, International Centre for Theoretical Physics, Trieste, Italy

Fred Kucharski

Earth System Physics Section, International Centre for Theoretical Physics, Trieste, Italy, and Center of Excellence for Climate Change Research/Department of Meteorology, King Abdulaziz University, Jeddah, Saudi Arabia

**Corresponding author address:* Giorgio Graffino, Earth System Physics Section, International Centre for Theoretical Physics, Strada Costiera 11, Trieste, Italy

E-mail: ggraffin@ictp.it

ABSTRACT

The importance of subtropical and extratropical zonal wind stress on Pacific Subtropical Cells (STCs) strength is assessed through several idealized numerical experiments performed with a global ocean model. Different zonal wind stress anomalies are employed, and their intensity is strengthened or weakened with respect to the climatological value throughout a suite of simulations. Strengthened (weakened) zonal wind stress anomalies result in increased (decreased) STCs meridional mass and energy transport. Upwelling of subsurface water into the tropics is intensified (reduced), a distinct cold (warm) anomaly appears in the equatorial thermocline and up to the surface, resulting in significant tropical sea surface temperature (SST) anomalies. Results hold for both subtropical and extratropical anomalies, suggesting the potential impact of mid-latitude atmospheric modes of variability on tropical climate. Finally, the remotely-driven response is compared with a set of locally-forced simulations, where an equatorial zonal wind stress anomaly is imposed. A dynamically distinct response is achieved, whereby the equatorial thermocline adjusts to the wind stress anomaly resulting in significant equatorial SST anomalies as in the remotely-forced simulations. Significant anomalies in the Indonesian throughflow are generated only when equatorial wind stress anomalies are applied, leading to remarkable heat content anomalies in the Indian Ocean. Equatorial wind stress anomalies experiments do not involve modifications of STC transports, but could set up the appropriate initial conditions for a tropical-extratropical teleconnection, involving both Hadley cells and STC anomalous transports.

1. Introduction

Among all the interaction mechanisms relating the equatorial ocean to the extratropical and sub-tropical regions, the SubTropical Cells (STCs) are of paramount importance.

Their existence in the Pacific Ocean was theoretized by several works during the 1990s (McCreary and Lu 1994; Liu 1994; Lu et al. 1998), and was supported by observational (McPhaden and Zhang 2002, 2004; Zhang and McPhaden 2006) and modelling studies (Klinger et al. 2002; Nonaka et al. 2002; Solomon et al. 2003). STCs are meridional overturning circulations involving the subtropical-tropical region. They are shallow, extending from the surface to about 500 m depth. In the time-mean, a pair of STCs develop on each side of the Equator, consisting of a subtropical subduction branch, an equatorward advection in the subsurface layers, a sloped uprising in the equatorial thermocline, and finally a poleward return flow at the surface (Schott et al. 2004). Some important structural differences arise between the time-mean and the seasonal circulations (Nakano et al. 1999; Jayne and Marotzke 2001).

The uprising component of the STC circulation involves the Equatorial UnderCurrent (EUC), which feeds the thermocline at the Equator. The temperature of EUC water is in the range of 15°-25°C, meaning that the main source region must be located between 20° and 40° (Wyrtki and Kilonsky 1984), even though local recirculation of tropical waters can contribute as well.

The pathway followed by subducted water parcels is different between the two hemispheres. In the Northern Hemisphere the equatorward advection is limited, due to the presence of a high potential vorticity (PV) ridge close to 9°N (Lu and McCreary 1995; McPhaden and Zhang 2002). The PV ridge causes the water to take a longer route to reach the Equator (Johnson and McPhaden 1999; Johnson 2001). Therefore, water flowing from the northern Pacific Ocean to the Equator is made of two components: the western boundary part, and the interior part. The splitting of the equatorward flow in two components occurs in the Southern Hemisphere as well, but to a lesser extent. Decadal variations of western boundary and interior components are almost out-of-phase, but STC variations are mainly locked to the interior component (Lee and Fukumori 2003).

Other overturning cells exist in the tropical region, such as the Tropical Cells (TCs). TCs are driven by the decrease of Ekman poleward transport occurring at about 5° off the Equator (Molinari et al. 2003). Despite their intensity, TCs are associated with a small meridional energy transport (Hazeleger et al. 2000), but force us to be cautious on the assessment of STC properties.

STCs exert a large impact on the tropical ocean, since they can act as “ocean tunnels” (Liu and Alexander 2007), for example by altering the energy transport in the subtropics (Klinger and Marotzke 2000) and driving thermal anomalies at the Equator (Farneti et al. 2014a). The effect of local equatorial wind stress forcing is also significant in driving equatorial anomalies (Nonaka et al. 2002), and the relative importance of local versus remote wind stress forcing should be quantified and their dynamics investigated. Furthermore, STCs have been used to explain some decadal-scale variability in the Pacific Ocean (Capotondi et al. 2005), due to their influence on ENSO (Kleeman et al. 1999) and their relation with the Pacific Decadal Oscillation (PDO) (Farneti et al. 2014b; Hong et al. 2014). For example, the transition between negative to positive PDO in the 1970s is related to a concomitant slowdown of the STCs (McPhaden and Zhang 2002), with a “rebound” in the 1990s after another reversal of the PDO phase (McPhaden and Zhang 2004). In particular, the first regime shift seems to be responsible for an increase of 0.8°C in the tropical Pacific Ocean sea surface temperature (SST) from the 1970s to the early 1990s (Zhang et al. 1997).

Schott et al. (2007) assimilation model reduced STC variations to only 40% of the value found by McPhaden and Zhang (2002), which however are reproduced again using a different forcing product (Schott et al. 2008). STC decadal variability can also be reproduced using both ocean-only (Farneti et al. 2014a) and coupled models (Solomon and Zhang 2006; Zhang and McPhaden 2006).

Gu and Philander (1997) exploited STCs dynamics to explain the propagation of SST anomalies from the extratropics to the equatorial regions (the so-called $\bar{v}T'$ mechanism), although observational studies (Deser et al. 1996; Schneider et al. 1999) suggested that temperature signals would decay quickly away from their source region. Another interpretation of the STCs observed influence on tropical dynamics was given by Kleeman et al. (1999), who suggested that subtropical wind stress forcing was able to alter the equatorial temperature structure, by changing the strength of those shallow meridional circulation structures (the so-called $v'\overline{T}$ mechanism).

Recently, England et al. (2014) linked STCs dynamics to the recent global warming slow-down, which happened concurrently with a negative phase of the Interdecadal Pacific Oscillation (IPO) (Power et al. 1999; Meehl et al. 2013), corresponding to a cool tropical Pacific Ocean and an enhanced trade winds forcing. By linearly increasing the zonal wind stress forcing on the Pacific Ocean between 45°N and 45°S, England et al. (2014) accounted for a substantial heat content increase in the Indo-Pacific Ocean below 125 m and a decrease above 125 m.

The two-layer model of McCreary and Lu (1994) shows that the strength of the STC is related to the zonal wind stress at a cutoff latitude for subtropical subduction, set to 18°. Thus, the amount of water reaching the Equator is mainly remotely determined at subtropical latitudes, which is consistent with Pedlosky (1987) model, and not locally driven by the equatorial upwelling as suggested by Bryan (1991). The role of subtropical and extratropical zonal wind stress on the STC forcing is explored in more detail by Klinger et al. (2002), using the same 3-1/2 model of Lu et al. (1998) on a simplified representation of the Pacific Ocean. Klinger et al. (2002) performed experiments using both steady and oscillatory forcing in different sectors of the Pacific Ocean, finding an almost linear relationship between the strength of the subtropical wind stress and the

STC transport in steady-state conditions. Klinger et al. (2002) also underline the role of high-latitude anomalies on the ocean state at the Equator. Furthermore, their oscillating experiments show that an “optimal” forcing time period must exist, giving the biggest equatorial response.

Using idealized wind stress patterns and intensities, at different latitudes ranging from equatorial to extratropical, we test here some of the previously proposed hypothesis. In particular, we aim to quantify the relative importance of equatorial, subtropical and extratropical wind stress on driving STC mass and energy transport anomalies, which is also strictly related to the possibility of driving temperature and circulation anomalies at the Equator.

The paper is organised as follows. In Section 2 the setup of our numerical experiments is detailed, results are described in Section 3. Discussions and conclusions are given in Section 4.

2. Model and Experiments

We employed the NOAA/GFDL Modular Ocean Model version 5 (MOM5; Griffies (2012)), a global-ocean, volume-conserving, primitive equations model. The horizontal resolution is $1^\circ \times 1^\circ$, with a finer discretization from 30°N to 30°S in the meridional direction. The model has 50 vertical levels in depth coordinates and 80 levels in potential density coordinates. Subgrid mesoscale processes are parameterized using the Gent-McWilliams skew-flux closure scheme (Gent and Mcwilliams 1990; Gent et al. 1995; Griffies 1998), and submesoscale eddy fluxes are parameterized following Fox-Kemper et al. (2008, 2011).

Boundary conditions are imposed at the sea surface, where a climatological forcing is applied, namely the CORE-I (Griffies et al. 2009) atmospheric state. It consists of a Normal Year Forcing (NYF), where the same seasonally-varying forcing is applied at every model year. No sea surface temperature restoring is used; we apply however a salinity restoring with a relaxation timescale of 60 days.

We performed a long control run in order to obtain a statistically stable mean state. After about 4000 years the model has adjusted in its deep layers, and standard metrics show little if no drift.

Starting from the last 200 years of the control run, we performed several perturbation experiments using time-constant wind stress anomalies, see Table 1. Each zonal wind stress anomaly used in the simulation is obtained as a fraction of the climatological value, and then added to or subtracted from the NYF field. Figure 1 shows the zonal averages of the zonal wind stress anomalies and the resulting wind stress curl. Zonal wind stress anomalies, superimposed on the NYF forcing, are chosen according to their geographical location, or by choosing a proper wind stress threshold (Figure 2). For each case, ten experiments are performed (Table 1). Anomalous forcing experiments are 20 years long, and we show results averaged over the last 5 years.

Our main purpose is to assess the effect of subtropical and extratropical wind stress on STCs dynamics, and how their transport modifications propagate and influence the equatorial state. We carried out similar analyses on a set of equatorial experiments, in order to have a direct comparison between locally- and remotely-forced perturbation anomalies.

a. Volume and energy flux diagnostics

We compute the total meridional volume transport (in Sverdrups; 1 Sv = 10^6 m^3 s^{-1}) as

$$\Psi(y,z) = -\int_{\lambda_1}^{\lambda_2} \mathrm{d}x \int_{-h}^{\eta} \mathrm{d}z' \, (v + v^*), \tag{1}$$

where λ_1, λ_2 define the longitudinal extension of the basin, h is the ocean's depth, η is the sea surface, and the transport includes both resolved v and parameterized v^* velocities. In most of our analysis, only the equatorward meridional transport are considered.

The meridional total energy transport (PW = 10^{15} W) is computed as anomaly of the control run value, namely

$$E_{TOT}(y) = \rho_0 C_\mathrm{p} \int_{\lambda_1}^{\lambda_2} \mathrm{d}x \int_{-h}^{\eta} \mathrm{d}z\,(vT - v_c T_c), \tag{2}$$

where ρ_0=1035.0 kg m^{-3} is the reference density, C_p=3992.1 J kg^{-1} °C^{-1} is the heat capacity for seawater at constant pressure (Griffies 2012), v is now the total meridional velocity component and T is potential temperature for the perturbation experiment, whereas v_c and T_c relates to the control run.

The above diagnostic produces the full energy flux anomaly in the chosen latitudinal range. In order to isolate the contribution from the STCs, the energy transport calculation proposed by Klinger and Marotzke (2000) is also used, and only zonal wind stress and SST values are needed. As shown in Section d, wind-driven meridional mass transports and meridional SST gradients are exploited to compute the meridional energy flux ascribed to STCs only.

Ocean heat content (J) is also evaluated as an anomaly. The computation is given by

$$OHC = \rho_0 C_\mathrm{p} \int\limits_{\lambda_1}^{\lambda_2} \mathrm{d}x \int\limits_{\phi_1}^{\phi_2} \mathrm{d}y \int\limits_{-h}^{\eta} \mathrm{d}z\,(T - T_c). \tag{3}$$

Finally, the Indonesian ThroughFlow (ITF) accounts for the exchange of water between Pacific and Indian basins. It is computed summing up the zonal transport crossing the passage between South Timor and Australia, and the meridional transport passing through Lombok and Ombai Straits.

3. Results

We designed these experiments to test the sensitivity of a time-constant zonal wind stress anomaly on the STCs, located at some specific latitudinal range. Thus, they are not meant to reproduce any observed variability, but rather to quantify and test the sensitivity of STCs to idealized forcing anomalies. Although the absolute value of the imposed surface anomalies lies between the observed variability at both subtropics and extratropics (not shown), their duration is not realistic and serves the purpose of testing different hypothesis.

a. Equatorial Anomalies

Ten experiments were performed imposing a zonal wind stress anomaly at the Equator (Figure 2, panel c). Five experiments have strengthened wind stress anomalies added on the climatological forcing in that region, five have instead weakened anomalies. The pattern extends from 8°N to 8°S in latitude and from 170°E to 100°W in longitude, with values smoothed linearly to zero. The shape is similar to the region defined by England et al. (2014) as the IPO-related contribution to the strengthened trade winds circulation in the Pacific Ocean. The equatorial experiments assess the impact of zonal wind stress anomalies at the Equator on the STCs.

Figure 3 shows the time series of equatorward mass transport at 9°N and 9°S, at the boundaries of the anomaly. The transport from each experiment is zonally-integrated on the whole Indo-Pacific basin, vertically-integrated in the first 1000 m, and finally subtracted from the control value. At 9°N, an increasing divergence of the equatorward mass transport from the control value is obtained as the magnitude of the zonal wind stress anomaly increases. Instead, at 9°S the behavior is more chaotic, probably due to the contribution of the Indian Ocean in the computation. In each case, the mass transport anomalies are less than a tenth of the control value.

Top panels in Figure 4 show the anomalous transports for some selected experiments. For convenience, we show only results for the strengthened anomalies. Even though the impact of the equatorial wind stress anomalies on the overturning circulation is significant, the signal is confined to 10°N-10°S and to a limited density range (1030-1032 kg/m^3), and thus does not involve the subtropics. An equatorially-confined wind stress anomaly, however strong, is only able to force local overturning structures very close to the Equator, such as the Tropical Cells, but not the STCs.

Meridional energy transport anomalies are restricted to a small latitudinal extent across the Equator (not shown). Since TCs act over a weak temperature gradient their energy transport is limited, even in the case of strong wind stress forcing.

A thermal response at the Equator is clearly shown in Figure 4 (central panels), larger in the western Pacific Ocean and with anomalies up to 3°C. As we will show later, these signals are different from a typical STCs response (see central panels in Figs. 8 and 11), being related to a local adjustment of the thermocline to the wind stress, not to a remote advection from the STCs. In fact, a stronger (weaker) zonal wind stress at the Equator pushes more (less) efficiently the surface water towards the west, and the equatorial thermocline tilt is enhanced (reduced). For strengthened wind stress anomalies, a steeper thermocline results in a warm anomaly in the west Pacific and a cold anomaly in the east Pacific.

The zonal velocity structure driven by the equatorial anomalies looks like a dipole. In Fig. 4 (bottom panels), positive (negative) velocity anomalies in the lower (upper) pycnocline are obtained from the strengthened experiments; the pattern is reversed for the weakened experiments (not shown).

At the surface, a typical La-Niña condition develops for strengthened anomalies (Figure 5), with a cold SST anomaly (up to 1°C) developing at end of the simulations along the Equator. Conversely, the weakened experiments build up an El-Niño SST pattern. This temperature response is quite remarkable, since the NYF atmospheric state at the surface is constantly dampening any ocean thermal anomaly, constraining the simulated SST through the climatological atmospheric state.

By changing the equatorial wind stress strength, we are also changing the mass transport across Indonesian straits (Fig. 6). The anomaly of the Indonesian ThroughFlow (ITF) transport for the strongest experiments is up to 2 Sv, or about 15% with respect to the control transport of 11-12 Sv. Furthermore, the strength of the transport anomaly is similar to what has been estimated by previous studies (Meyers 1996; England and Huang 2005). It also explains the different behavoir between the STCs mass transport time series in the Northern Hemisphere (Fig. 3, left panel) and in the Southern Hemisphere (Fig. 3, right panel), being the latter estimate affected by the Indian Ocean contribution. As soon as the wind stress anomaly sets on, the ITF transport is modified with little delay. Then, it decays for some time before stabilization.

b. Subtropical Anomalies

The main STCs driving mechanism occurs through changes of the wind stress at the subtropics (McCreary and Lu 1994). Therefore, we expect the STCs response to be the largest when a wind stress anomaly is located in those regions. We performed twenty experiments (ten in each hemisphere), employing both strengthened and weakened anomalies (Figure 2a, d).

As shown in Figure 7, the effect of the subtropical anomalies is large on the STCs mass transport, up to 10-12 Sv for the strongest experiments at 15° in each hemisphere; at its maximum, the anomalous transport is roughly one third of the control value for both hemispheres. The stabilization of the trends occur on a decadal time scale, and is faster for the Northern Hemisphere experiments.

Some examples of the structure of the STCs response is shown in Figure 8. Compared to the equatorial anomalies (Figure 4), here we can see a proper response of the STCs involving the whole overturning structure from the Equator to the subtropical region. Only the Northern Hemisphere experiments are shown, the response of the Southern Hemisphere being very similar.

A broad meridional ocean energy transport anomaly, straddling the whole subtropical and tropical regions, is obtained for both Northern and Southern Hemisphere experiments (not shown). The anomalous energy transport spans the whole subtropical region, with anomalies ranging from 0.03 PW (10% of the control value) for the 10% experiment to 0.3 PW (60% of the control value) for the 50% experiment. It should be noted that the computation includes the Indian Ocean transport, affecting the Southern Hemisphere estimate. A linear relationship between meridional energy transport and wind stress holds, mainly for small anomalies. For larger anomalies (40% and 50%) this relationship is lost. In fact, large wind stress anomalies are affecting not only the STCs, but significantly modify energy transports related to the wind-driven gyre.

By changing the STCs transport, subtropical wind stress anomalies are able to drive a considerable response at the Equator (Figure 8, central and bottom panels). Comparing our subtropical results with the equatorial ones (Figure 4), we can see how the two responses are significantly different. In the equatorial experiments, even though the thermal signal can be stronger locally, as in the west Pacific, we do not see any STC-related effect. Instead, cold anomalies arising in the equatorial thermocline from the strengthened subtropical wind stress anomalies can be traced to a remote response due to the STCs (Figure 8). Indeed, an accelerated STC is able to draw deeper (and colder) water to the Equator, by feeding the EUC (Fig. 8, bottom panels). Similarly, weakened subtropical wind stress anomalies drive warm anomalies at Equator by slowing the EUC and reducing the local upwelling of relatively cold waters.

Looking at the sea surface (Figure 9), a cold SST signature develops from the 20% strengthened experiment onwards. A warm response is instead obtained in the weakened experiments (not shown). Considering only the north-subtropical experiments, both strengthened and weakened 50% wind stress anomalies drive a response up to 0.48°C in the Niño 3.4 region. South-subtropical experiments drive a slightly smaller thermal signal. These values are very close to the threshold

(0.5°C, https://www.ncdc.noaa.gov/teleconnections/enso/indicators/sst.php) associated to a warm or cold ENSO phase.

There is no significant anomaly in the ITF transport in any of the subtropical experiments (not shown). This result indicates that strengthening or weakening the STC transport does not lead to any appreciable modification of the ITF mass transport.

c. Extratropical Anomalies

We showed how a subtropical zonal wind stress anomaly can influence the STC dynamics. Now, our purpose is to verify whether such influence could occur with an anomaly located further poleward. Indeed, many mid-latitude weather regimes are related with characteristic zonal wind stress patterns in the Pacific sector. The following experiments test if there can be a teleconnection between mid-latitude wind stress anomalies and the equatorial ocean through ocean dynamics.

We performed twenty experiments imposing two idealized extratropical anomalies (Figure 2b, e). Anomalies extended from 15° to 45° in each hemisphere, with a 10-step linear smoothing. As before, the intensity of the anomaly was a fraction of the climatological zonal wind stress (Table 1).

Figure 10 shows the time series of the equatorward STCs mass transport computed at 20° for each hemisphere. Transport anomalies are weaker than their subtropical counterparts (Figure 7). Furthermore, full equilibration to a new time-mean transport is not achieved during the length of the simulation, and some experiments do oscillate within 2-3 Sv of amplitude. Because of their location, mid-latitude wind stress anomalies need a longer time to influence the oceanic meridional overturning circulation and to reach an equilibrated state. Nevertheless, mass transport anomalies forced by the strongest experiments are more than half of the control value.

As seen in Figure 11 (top panels), there is a significant STC anomalous transport which is able to propagate towards the Equator for the strongest experiment (Figure 8). Hence, a distinct STC response can be generated even with an extratropical forcing.

Given the weaker dynamical response with extratropical forcing, ocean energy transport anomalies are also smaller than those produced by subtropical wind stress anomalies, and values are closer to the control state (not shown). Energy transport anomalies range from 0.01 PW to 0.1 PW, roughly half of the subtropical response. The largest energy transport anomalies are roughly 25% of the control value in the Northern Hemisphere and 10% in the Southern Hemisphere.

A thermal response at the Equator is also generated (Figure 11). Comparing with the subtropical experiments (Figure 8), now temperature anomalies (up to 0.7°C) are more localized within the thermocline with respect to their subtropical counterpart, but weaker in intensity.

Equatorial SST shows a remarkable cold anomaly for the strongest experiments in the eastern Pacific Ocean (Figure 12). In the 50% strengthened experiment, a cold anomaly of 0.27°C develops before the end of the simulation, whereas a warm anomaly of 0.14°C holds in the 50% weakened experiment.

d. Meridional energy transport by the STC

The meridional energy transport calculations presented so far included all dynamical processes, which in the Pacific mainly involves the STCs and the wind-driven gyre contributions. In order to isolate the STCs contribution we employed the method developed by Klinger and Marotzke (2000), which allows the computation of the STC-related meridional energy transport using Ekman dynamics. The expression for the STC meridional energy transport is

$$\mathrm{E_{STC}}(y) = C_\mathrm{p} \int_{\lambda_1}^{\lambda_2} \mathrm{d}x \int_{y_1}^{y} \mathrm{M_E} \frac{\partial \theta}{\partial y} \, \mathrm{d}y, \tag{4}$$

where $M_E = -\tau(y)/f(y)$ is the Ekman mass transport and θ the surface potential temperature. The energy transport is integrated zonally and for each model grid point between 10° and the latitude of zero wind stress (≈30°). A full derivation of Eq. 4 is provided in the Appendix.

We first reproduced the estimates for the STC meridional energy transport in our control run for all basins (Fig. 13). Our model results compare well with the observational estimates given in Klinger and Marotzke (2000, c.f. Fig. 6). Because of their zonal extent, Pacific and Indian Ocean STCs stand out with the largest meridional fluxes.

In Fig. 14 we compute STCs meridional energy transport anomalies generated by the equatorial, northern subtropical and northern extratropical wind stress anomalies. As expected, equatorial experiments produce very weak anomalies (Figure 14a, d), close to zero with some significant deviations from the control state within the equatorial region. Subtropical (Fig. 14b, e) and extratropical (Fig. 14c, f) experiments are instead associated with large STC meridional energy transport anomalies, extending up to 20° and 25° for the subtropical and extratropical wind stress forcing, respectively. Meridional energy transport anomalies directly related to STCs account for ≈1/3 of the total anomaly. The relative role of STCs is larger for modest anomalies, whereas it becomes less important for the strongest cases. This is probably due to the intensification of the wind-driven subtropical gyre, transporting large amount of heat poleward. Furthermore, in the Northern Hemisphere the STC energy transport anomalies for the extratropical experiments are larger than their subtropical counterparts. It is probably related to the different shape of the wind stress anomalies, which is very localized for the subtropical case (Fig. 2a). In the Southern Hemisphere, in which basin-wide wind stress anomalies are employed (Fig. 2d, e), the subtropical experiments give larger energy transport than the extratropical ones.

4. Discussions and conclusions

We studied the effect of different wind stress patterns, located in different areas of the Pacific Ocean, on the Pacific SubTropical Cells (STCs). Employing a global ocean model (MOM5; Griffies (2012)), we applied idealized time-invariant zonal wind stress anomalies at the sea surface, strengthening or weakening the climatological forcing. We note that the observed interannual variability of the zonal wind stress in Pacific extratropical regions can produce anomalies even larger than the one used in this study. Analyzing the 60-years-long CORE-II dataset (Griffies et al. 2009), we find that the variance of the zonal wind stress in the extratropics in the Northern Pacific Ocean can be even larger than 50% of the mean value (not shown). Results from the different perturbation experiments are compared with respect to a climatologically-forced long control run.

In England et al. (2014) a zonal wind stress anomaly was applied to the entire Pacific basin from 45°N to 45°S. We chose a different approach, generating a STC response by selecting a particular forcing location, in order to maximize the signal. In general, the local response at the Equator produced by trade winds anomalies is stronger than the one generated from outside the tropics. In fact, by changing the wind stress forcing on a very large area, the biggest part of the subtropical and extratropical signal could be lost. Indeed, the structure of the meridional overturning circulation trend in England et al. (2014) is very similar, in terms of spatial extension, to what is obtained here with equatorial wind stress anomalies (Figure 4).

Our results can be summarized as follows.

- Equatorial wind stress anomalies located between 8°S and 8°N do not extend poleward enough in order to force the STCs. Zonal cross sections at the Equator showed large thermal anomalies (up to 3°C) in some cases, but they are related to an adjustment of the thermocline in response to the different local wind stress forcing. Appreciable changes in ITF transport are also obtained (up to 2 Sv), leading to a remarkable temperature anomaly in the Indian Ocean (not shown).

- Among all experiments, subtropical wind stress anomalies have the strongest impact on STCs. Equatorward mass transport anomalies reach 12 Sv, roughly one third of the control value. The excited STCs motion develops mainly in the thermocline, with a striking thermal signal appearing at the Equator: up to 1°C at depth and 0.5°C at the surface. In terms of energy transport, anomalies reach more than half of the control value for the strongest experiment. However, if a diagnostic for STC-related meridional energy transport is used, then STCs account for about $\approx$1/3 of the total transport anomaly.

- Extratropical wind stress anomalies also generate a significant influence on both mass and energy STCs transport, with weaker anomalies compared to subtropical experiments. A full stabilization of the trend of some experiments is not achieved during the 20 years simulation. However, the anomalous mass transport is more than half of the control value in the strongest experiments, with the STC-related meridional energy transport accounting for more than half of the total transport. A remarkable thermal signal is forced at the Equator, with anomalies of 0.7°C in the thermocline and 0.3°C at sea surface.

The overall behavior of the northern-hemisphere experiments is summarized in Figure 15, where values of anomalous wind stress forcing are plotted against anomalies in equatorward mass transport, STC energy transport and equatorial SST.

Equatorial experiments are not able to drive a substantial response in terms of mass and energy transport. In fact, however strong, equatorial wind stress anomalies are always related to a local recirculation of the surface waters, with a thermal signal due to the the adjustment of the thermocline to the changing wind stress at the surface. Thus, here only the shallower Tropical Cells are excited. Even though the equatorial wind stress anomalies experiments do not involve modifications of STC transports, they could set up the appropriate initial conditions for a tropical-extratropical teleconnection, involving both Hadley cells and STC anomalous transports, as hypothesized in Farneti et al. (2014a). In any case, SST anomalies in the Niño 3.4 region are higher for the equatorial experiments, stressing the importance of the local wind stress forcing on the equatorial ocean state. Despite the climatological atmospheric surface temperature applied by the model at the sea surface, remotely-induced thermal anomalies in the equatorial thermocline are able to propagate to the surface, with values up to 0.5°C in the central Pacific Ocean. These values are comparable with those found by Farneti et al. (2014a) using an OGCM forced by CORE-II reanalyses.

Regarding both STC mass and energy transports, the strongest values are obtained with subtropical wind stress anomalies, although extratropical mass transports are almost comparable. Overall, subtropical zonal wind stress anomalies were found to be the strongest forcing mechanism of the STCs in the Pacific Ocean, as predicted by previous theoretical studies (e.g. McCreary and Lu 1994). However, we showed that extratropical wind stress anomalies are also capable of driving a substantial response in the overturning cells, especially for the experiments with a large forcing (30% to 50% of the climatological value).

Overall, the good agreement between the regression lines and our key metrics in Fig. 15 suggests the possibility of a linear relationship with the applied wind stress forcing. Thus, together with the linear fits, angular coefficients are shown for each regression line. Subtropical and extratropical experiments shows a good agreement between strengthened and weakened experiments, in both equatorward mass transport and STC energy transport. Instead, equatorial SST does not show similar behaviors for strengthened and weakened experiments, making harder the interpretation of the STCs influence on SST in terms of linear response.

Among the different processes connecting the tropical to the subtropical ocean, our experiments suggest that the Kleeman et al. (1999) hypothesis is the most reliable. An anomalous STC transport drives a surface thermal signal at the Equator by modifying the feeding of subsurface water to the thermocline. Our subtropical and extratropical experiments drive a substantial STC response in the equatorial thermocline, where the bulk of the Equatorial Undercurrent flows and forms part of the returning branch of the STC circulation.

Indeed, ocean heat content anomalies in the equatorial Pacific Ocean (10°N-10°S), integrated at different depths during the final stage of the simulation for strengthened experiments (see Tab. 2), show a strong heat content increase in the first 300 m for the equatorial set, accounting for the whole increase in the total ocean column. Furthermore, the ITF advects part of the generated signal into the Indian Ocean, leading to significant heat content anomalies in the first 1000 m for all equatorial experiments (not shown). For subtropical experiments a negative heat content anomaly is generated, since a strengthened STC circulation draws deeper (and colder) water to the surface, as shown in Fig. 8. Again, the heat content change is mostly located in upper 300 meters. Extratropical wind stress anomalies also result in a reduction of heat content in the upper layers, although much reduced in terms of magnitude.

Our experimental set-up proved very useful in highlighting some fundamental properties of STC dynamics and its connection to the tropical ocean. However, we acknowledge the idealized nature of our modelling framework. In particular, the time-independent wind stress anomalies applied and the absence of ocean-atmosphere coupling are among the strongest limitations of our study. A followed-up study will use observed wind stress patterns, with both time-constant and time-evolving anomalies. The implementation of a set of experiments using time-evolving wind stress anomalies will be important in order to increase our understanding about the time scales and transient phases in STC response.

Acknowledgments. Thanks to the Center of Excellence for Climate Change Research (KAU University) for providing funds for this publication. The CORE datasets are collaboratively supported by the National Center for Atmospheric Research (NCAR) and the Geophysical Fluid Dynamics Laboratory (GFDL) under the umbrella of the Climate Variability and Predictability (CLIVAR) Working Group on Ocean Model Development (WGOMD). All datasets, codes for the bulk formulas, technical report, and other support codes along with the release notes are freely available at http://data1.gfdl.noaa.gov/nomads/forms/core.html.

APPENDIX

Meridional energy transport by the SubTropical Cells

The momentum balance in the Ekman boundary layer is expressed as Vallis (2006)

$$f\,\mathbf{k}\times\mathbf{u}_{\mathrm{E}} = \frac{1}{\rho_0}\frac{\partial \boldsymbol{\tau}}{\partial z}, \tag{A1}$$

where f is the Coriolis parameter, $\mathbf{u}_{\mathrm{E}}$ is the horizontal velocity vector in the Ekman layer, $\boldsymbol{\tau}$ the surface wind stress, ρ_0 a reference density and $\mathbf{k}$ the unit vertical direction.

Vertically integrating Eq. A1 yields

$$f\,\mathbf{k}\times\mathbf{M}_{\mathrm{E}} = \boldsymbol{\tau}, \tag{A2}$$

and the integrated mass transport in the Ekman layer is

$$\mathbf{M}_{\mathrm{E}} = \int_{-h}^{0} \rho_0\mathbf{u}_{\mathrm{E}}\,\mathrm{d}z = \frac{\boldsymbol{\tau}\times\mathbf{k}}{f}, \tag{A3}$$

where $z=-h$ is the characteristic depth of the Ekman layer and Eq. A3 defines the Ekman transport to be proportional to the magnitude of the wind stress.

Suppose now the wind stress to be zonal $\tau(y)$, providing a meridional mass flux $\mathrm{M}_{\mathrm{E}} = -\tau(y)/f(y)$. The wind stress τ is a function of latitude, generating a flow divergence at the surface and implying subduction into the ocean interior. Over a latitudinal interval δy, and using mass conservation, the mass flux subducted $\mathrm{M_S}$ is

$$\mathrm{M_S} = \frac{\partial \mathrm{M_E}}{\partial y} \delta y. \tag{A4}$$

If a latitude at which $\tau = 0$ exists, as observed, then mass conservation requires all Ekman mass flux to be subducted. The flow beneath the Ekman layer exactly balances the mass flux in the Ekman layer, and the subducted mass flux $\mathrm{M_S}$ is equal and opposite to the Ekman mass flux $\mathrm{M_E}$. Considering a full latitudinal extent

$$\mathrm{M_S} = \int_{y}^{y_1} \frac{\partial \mathrm{M_E}}{\partial y} \,\mathrm{d}y = -\mathrm{M_E}(y), \tag{A5}$$

where y_1 is a subtropical subduction latitude at which $\tau = 0$ and we have noted that $\mathrm{M_E}(y_1) = 0$.

The temperature of the Ekman flow is $\theta(y)$, whereas the subducted flow conserves the surface temperature $\theta(y_1)$, assuming an interior adiabatic flow. The temperature flux associated with the Ekman flow is thus $\mathrm{T}_E(y) = \theta(y)\mathrm{M_E}$, whereas the returning branch of the circulation has a temperature flux given by

$$\mathrm{T}_S(y) = -\int_{y}^{y_1} \theta(y) \frac{\partial \mathrm{M_E}}{\partial y} \,\mathrm{d}y. \tag{A6}$$

The net temperature flux, which we relate to the STC, is given by Klinger and Marotzke (2000) and Held (2001) as

$$\begin{aligned} \mathrm{T_{STC}}(y) &= \theta(y)\mathrm{M_E} + \int_{y}^{y_1} \theta(y) \frac{\partial \mathrm{M_E}}{\partial y} \,\mathrm{d}y && \text{(A7)} \\ &= -\int_{y}^{y_1} \mathrm{M_E} \frac{\partial \theta}{\partial y} \,\mathrm{d}y = \int_{y}^{y_1} \frac{\tau(y)}{f} \frac{\partial \theta}{\partial y} \,\mathrm{d}y. && \text{(A8)} \end{aligned}$$

Or, in θ-space

$$\mathrm{T_{STC}}(y) = -\int_{y}^{y_1} \mathrm{M_E} \frac{\partial \theta}{\partial y} \,\mathrm{d}y = \int_{y_1}^{y} \mathrm{M_E} \frac{\partial \theta}{\partial y} \,\mathrm{d}y = \int_{\theta(y_1)}^{\theta(y)} \mathrm{M_E} \,\mathrm{d}\theta. \tag{A9}$$

The last expression is the same as Eq. 11 in Klinger and Marotzke (2000) and Eq. 8 in Held (2001).

The meridional energy transport of the subtropical cell is obtained by zonally integrating the temperature flux and multiplying by C_p, the heat capacity of the ocean

$$\mathrm{E}_{\mathrm{STC}}(y) = C_\mathrm{p} \int_{\lambda_1}^{\lambda_2} \mathrm{d}x \int_{y_1}^{y} \mathrm{M}_\mathrm{E} \frac{\partial \theta}{\partial y} \, \mathrm{d}y. \tag{A10}$$

References

Bryan, K., 1991: Poleward heat transport in the ocean: A review of a hierarchy of models of increasing resolution. *Tellus*, **43 (4)**, 104–115, doi:10.3402/tellusa.v43i4.11940.

Capotondi, A., M. Alexander, C. Deser, and M. McPhaden, 2005: Anatomy and decadal evolution of the Pacific Subtropical-Tropical Cells (STCs). *J. Climate*, **18 (18)**, 3739–3758.

Deser, C., M. Alexander, and M. Timlin, 1996: Upper-ocean thermal variations in the North Pacific during 1970-1991. *J. Climate*, **9 (8)**, 1840–1855.

England, M., and F. Huang, 2005: On the interannual variability of the Indonesian Throughflow and its linkage with ENSO. *J. Climate*, **18 (9)**, 1435–1444.

England, M., S. McGregor, P. Spence, G. Meehl, A. Timmermann, . W. Cai, and A. Santoso, 2014: Recent intensification of wind-driven circulation in the Pacific and the ongoing warming hiatus. *Nature Clim. Change*, **4 (3)**, 222–227.

Farneti, R., S. Dwivedi, F. Kucharski, F. Molteni, and G. Griffies, 2014a: On Pacific Subtropical Cell variability over the second half of the twentieth century. *J. Climate*, **27**, 71027112, doi: 10.1175/JCLI-D-13-00707.1.

Farneti, R., F. Molteni, and F. Kucharski, 2014b: Pacific interdecadal variability driven by tropical-extratropical interactions. *Clim. Dyn.*, **42 (11-12)**, 3337–3355.

Fox-Kemper, B., R. Ferrari, and R. Hallberg, 2008: Parameterization of mixed layer eddies. Part I: Theory and diagnosis. *J. Phys. Oceanogr.*, **38**, 11451165, doi:10.1175/2007JPO3792.1.

Fox-Kemper, B., and Coauthors, 2011: Parameterization of mixed layer eddies. Part III: Implementation and impact in global ocean climate simulations. *Ocean Modelling*, **39**, 61–78, URL https://doi.org/10.1016/j.ocemod.2010.09.002.

Gent, P., and J. Mcwilliams, 1990: Isopycnal mixing in ocean circulation models. *J. Phys. Oceanogr.*

Gent, P., J. Willebrand, T. McDougall, and J. McWilliams, 1995: Parameterizing eddy-induced tracer transports in ocean circulation models. *J. Phys. Oceanogr.*, **25**, 463474, doi:10.1175/1520-0485(1995)025⟨0463:PEITTI⟩2.0.CO;2.

Griffies, S., 1998: The Gent-McWilliams skew flux. *J. Phys. Oceanogr.*, **28**, 831841, doi:10.1175/1520-0485(1998)028⟨0831:TGMSF⟩2.0.CO;2.

Griffies, S., 2012: *Elements of the Modular Ocean Model (MOM)*. Princeton (NJ), USA, NOAA Geophysical Fluid Dynamics Laboratory.

Griffies, S., A. Biastoch, C. Bning, F. Bryan, G. Danabasoglu, E. C. ..., and W. Hazeleger, 2009: Coordinated Ocean-ice Reference Experiments (COREs). *Ocean Modelling*, **26 (1)**, 1–46.

Gu, D., and S. Philander, 1997: Interdecadal climate fluctuations that depend on exchanges between the tropics and extratropics. *Science*, **275 (5301)**, 805–807.

Hazeleger, W., P. de Vries, and G. van Oldenborgh, 2000: Do Tropical Cells ventilate the Indo-Pacific equatorial thermocline? *Geophys. Res. Lett.*, **28 (9)**, 1763–1766.

Held, I., 2001: The partitioning of the poleward energy transport between the tropical ocean and atmosphere. *J. Atmos. Sci.*, **58**, 943948, doi:10.1175/1520-0469(2001)058⟨0943:TPOTPE⟩2.0.CO;2.

Hong, L., L. Zhang, Z. Chen, and L. Wu, 2014: Linkage between the Pacific Decadal Oscillation and the low frequency variability of the Pacific Subtropical Cell. *J. Geophys. Res.: Oceans*, **119**, 34643477, doi:10.1002/2013JC009650.

Jayne, S., and J. Marotzke, 2001: The dynamics of ocean heat transport variability. *Rev. Geophys.*, doi:10.1029/2000RG000084.

Johnson, G., 2001: The Pacific Ocean Subtropical Cell surface limb. *Geophys. Res. Lett.*, **28 (9)**, 1771–1774, doi:10.1029/2000GL012723.

Johnson, G., and M. McPhaden, 1999: Interior pycnocline flow from the subtropical to the equatorial Pacific Ocean. *J. Phys. Oceanogr.*, **29 (12)**, 3073–3089.

Kleeman, R., J. McCreary, and B. Klinger, 1999: A mechanism for generating ENSO decadal variability. *Geophys. Res. Lett.*, **26 (12)**, 1743–1746.

Klinger, B., and J. Marotzke, 2000: Meridional heat transport by the Subtropical Cell. *J. Phys. Oceanogr.*, **30 (4)**, 696–705.

Klinger, B., J. McCreary, and R. Kleeman, 2002: The relationship between oscillating subtropical wind stress and equatorial temperature. *J. Phys. Oceanogr.*, **32**, 15071521, doi: 10.1175/1520-0485(2002)032⟨1507:TRBOSW⟩2.0.CO;2.

Lee, T., and I. Fukumori, 2003: Interannual-to-decadal variations of tropical-subtropical exchange in the Pacific Ocean: Boundary versus interior pycnocline transports. *J. Climate*, **16**, 40224042, doi:10.1175/1520-0442(2003)016⟨4022:IVOTEI⟩2.0.CO;2.

Liu, Z., 1994: A simple model of the mass exchange between the subtropical and tropical ocean. *J. Phys. Oceanogr.*, **24 (6)**, 1153–1165.

Liu, Z., and M. Alexander, 2007: Atmospheric bridge, oceanic tunnel, and global climatic teleconnections. *Rev. Geophys.*, doi:10.1029/2005RG000172.

Lu, P., and J. McCreary, 1995: Influence of the ITCZ on the flow of thermocline water from the subtropical to the equatorial Pacific Ocean. *J. Phys. Oceanogr.*, **25**, 30763088, doi:10.1175/1520-0485(1995)025⟨3076:IOTIOT⟩2.0.CO;2.

Lu, P., J. McCreary, and B. Klinger, 1998: Meridional circulation cells and the source waters of the Pacific Equatorial Undercurrent. *J. Phys. Oceanogr.*, **28 (1)**, 62–84.

McCreary, J., and P. Lu, 1994: Interaction between the subtropical and equatorial ocean circulations: The Subtropical Cell. *J. Phys. Oceanogr.*, **24 (2)**, 466–497.

McPhaden, M., and D. Zhang, 2002: Slowdown of the meridional overturning circulation in the upper Pacific Ocean. *Nature*, **415 (6872)**, 603–608.

McPhaden, M., and D. Zhang, 2004: Pacific Ocean circulation rebounds. *Geophys. Res. Lett.*, **31**, doi:10.1029/2004GL020727.

Meehl, G. A. H. J. A., J. Fasullo, and K. Trenberth, 2013: Externally forced and internally generated decadal climate variability associated with the Interdecadal Pacific Oscillation. *J. Clim.*, **26 (18)**, 7298–7310, doi:10.1175/JCLI-D-12-00548.1.

Meyers, G., 1996: Variation of Indonesian Throughflow and the El Niño Southern Oscillation. *J. Geophys. Res.: Oceans*, **101 (C5)**, 12 255–12 263.

Molinari, R., S. Bauer, D. Snowden, G. J. B. Bourles, Y. Gouriou, and H. Mercier, 2003: A comparison of kinematic evidence for Tropical Cells in the Atlantic and Pacific Oceans. *Elsevier Ocean. Ser.*, **68**, 269–286.

Nakano, H., R. Furue, and N. Suginohara, 1999: Effect of seasonal forcing on global circulation in a World Ocean general circulation model. *Clim. Dyn.*, **15 (7)**, 491–502, doi:10.1007/s003820050295.

Nonaka, M., S. Xie, and J. McCreary, 2002: Decadal variations in the Subtropical Cells and equatorial Pacific sst. *Geophys. Res. Lett.*, **29 (7)**, doi:10.1029/2001GL013717.

Pedlosky, J., 1987: An inertial theory of the Equatorial Undercurrent. *J. Phys. Oceanogr.*, **17**, 19781985, doi:10.1175/1520-0485(1987)017⟨1978:AITOTE⟩2.0.CO;2.

Power, S., T. Casey, C. Folland, A. Colman, and V. Mehta, 1999: Inter-decadal modulation of the impact of ENSO on Australia. *Clim. Dyn.*, **15 (5)**, 319–324, doi:10.1007/s003820050284.

Schneider, N., A. M. M. Alexander, and C. Deser, 1999: Subduction of decadal North Pacific temperature anomalies: Observations and dynamics. *J. Phys. Oceanogr.*, **29 (5)**, 1056–1070.

Schott, F., J. McCreary, and G. Johnson, 2004: *Earth's Climate*, chap. Shallow Overturning Circulations of the Tropical-Subtropical Oceans. American Geophysical Union, Washington, D.C., USA, doi:10.1029/147GM15.

Schott, F., L. Stramma, W. Wang, B. Giese, and R. Zantopp, 2008: Pacific Subtropical Cell variability in the SODA 2.0.2/3 assimilation. *Geophys. Res. Lett.*, **35**, L10 607, doi:10.1029/2008GL033757.

Schott, F., W. Wang, and D. Stammer, 2007: Variability of Pacific Subtropical Cells in the 50-year ECCO assimilation. *Geophys. Res. Lett.*, **34**, L05 604, doi:10.1029/2006GL028478.

Solomon, A., J. McCreary, R. Kleeman, and B. Klinger, 2003: Interannual and decadal variability in an intermediate coupled model of the Pacific region. *J. Climate*, **16**, 383405, doi:10.1175/1520-0442(2003)016⟨0383:IADVIA⟩2.0.CO;2.

Solomon, A., and D. Zhang, 2006: Pacific subtropical cell variability in coupled climate model simulations of the late 19th20th century. *Ocean Modelling*, **15**, 236–249, doi:10.1016/j.ocemod.2006.03.007.

Vallis, G., 2006: *Atmospheric and oceanic fluid dynamics*. Cambridge Univ. Press. 745 pp.

Wyrtki, K., and B. Kilonsky, 1984: Mean water and current structure during the Hawaii-to-Tahiti Shuttle Experiment. *J. Phys. Oceanogr.*, **14**, 242254, doi:10.1175/1520-0485(1984)014⟨0242:MWACSD⟩2.0.CO;2.

Zhang, D., and M. McPhaden, 2006: Decadal variability of the shallow Pacific meridional overturning circulation: Relation to tropical sea surface temperatures in observations and climate change models. *Ocean Modelling*, **15 (3)**, 250–273, doi:10.1016/j.ocemod.2005.12.005.

Zhang, Y., J. Wallace, and D. Battisti, 1997: ENSO-like interdecadal variability: 1900-93. *J. Climate*, **10 (5)**, 1004–1020.

LIST OF TABLES

TABLE 1. Main characteristics of the perturbation experiments. τ_x is the zonal wind stress applied to the ocean surface during each experiment. The ocean model computes the zonal wind stress from the climatological zonal wind (NYF). Then, during the perturbation experiments, an anomaly is added to the climatological wind stress as a fraction, positive or negative, of the wind stress itself.

Experiment	τ_x	Time (years)
Control	NYF	1400
10	NYF$\pm$10%	20
20	NYF$\pm$20%	20
30	NYF$\pm$30%	20
40	NYF$\pm$40%	20
50	NYF$\pm$50%	20

TABLE 2. Ocean heat content anomaly (10^{21} J) in the equatorial Pacific Ocean (10°N-10°S) resulting from equatorial, north subtropical, and north extratropical strengthened experiments. Values are given for the upper 300 m, upper 1000 m and the total water column. Only the weakest and strongest wind stress anomaly experiments are considered.

	Equatorial		Subtropical		Extratropical	
Depth	10%	50%	10%	50%	10%	50%
0 - 300 m	154	717	-52.5	-275	-20.1	-93
0 - 1000 m	153	717	-56	-284	-16.3	-77.4
Total	153	717	-55.5	-280	-15.9	-67.6

LIST OF FIGURES

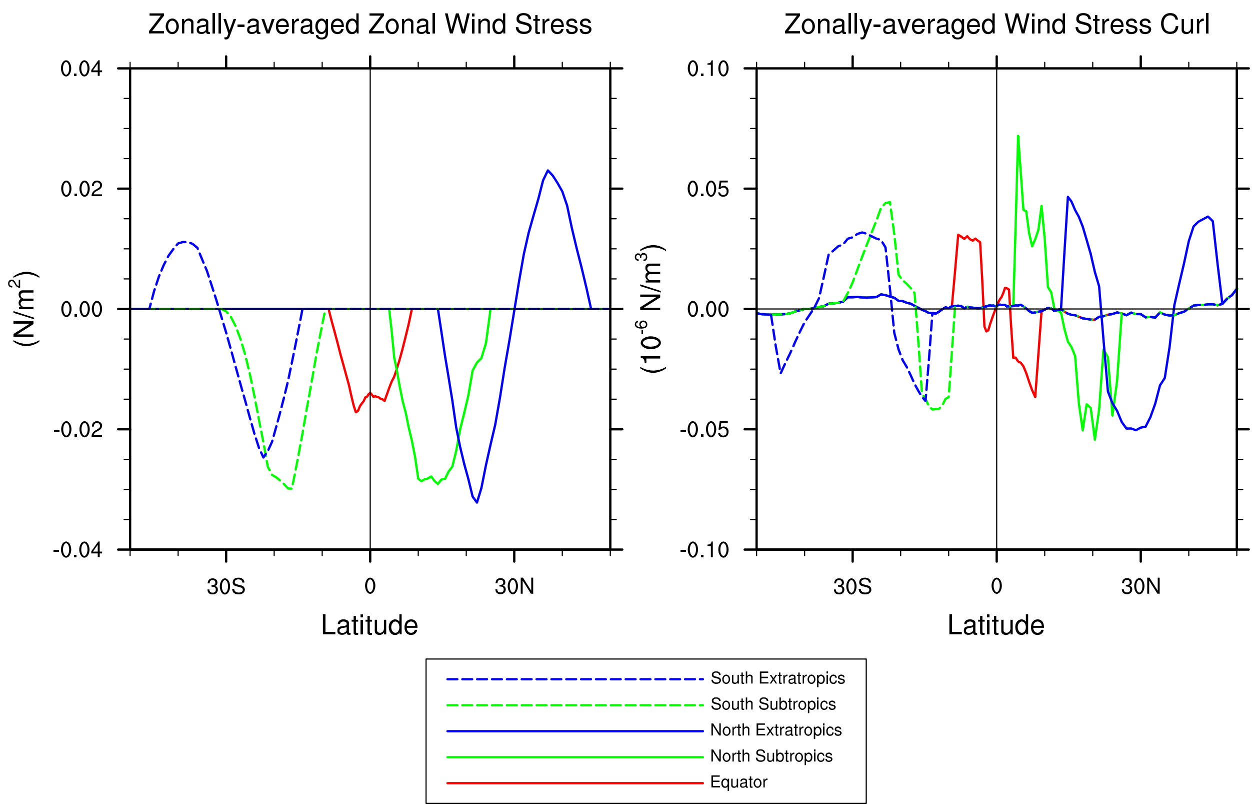

FIG. 1. Zonal average of the zonal wind stress anomalies (N/m^2, left panel) and resulting wind stress curl anomalies (10^{-6} N/m^3, right panel), computed from the climatological value of the zonal wind stress from the CORE-I dataset (Griffies et al. 2009). Each anomaly is added or subtracted to the NYF, after been multiplied by a factor.

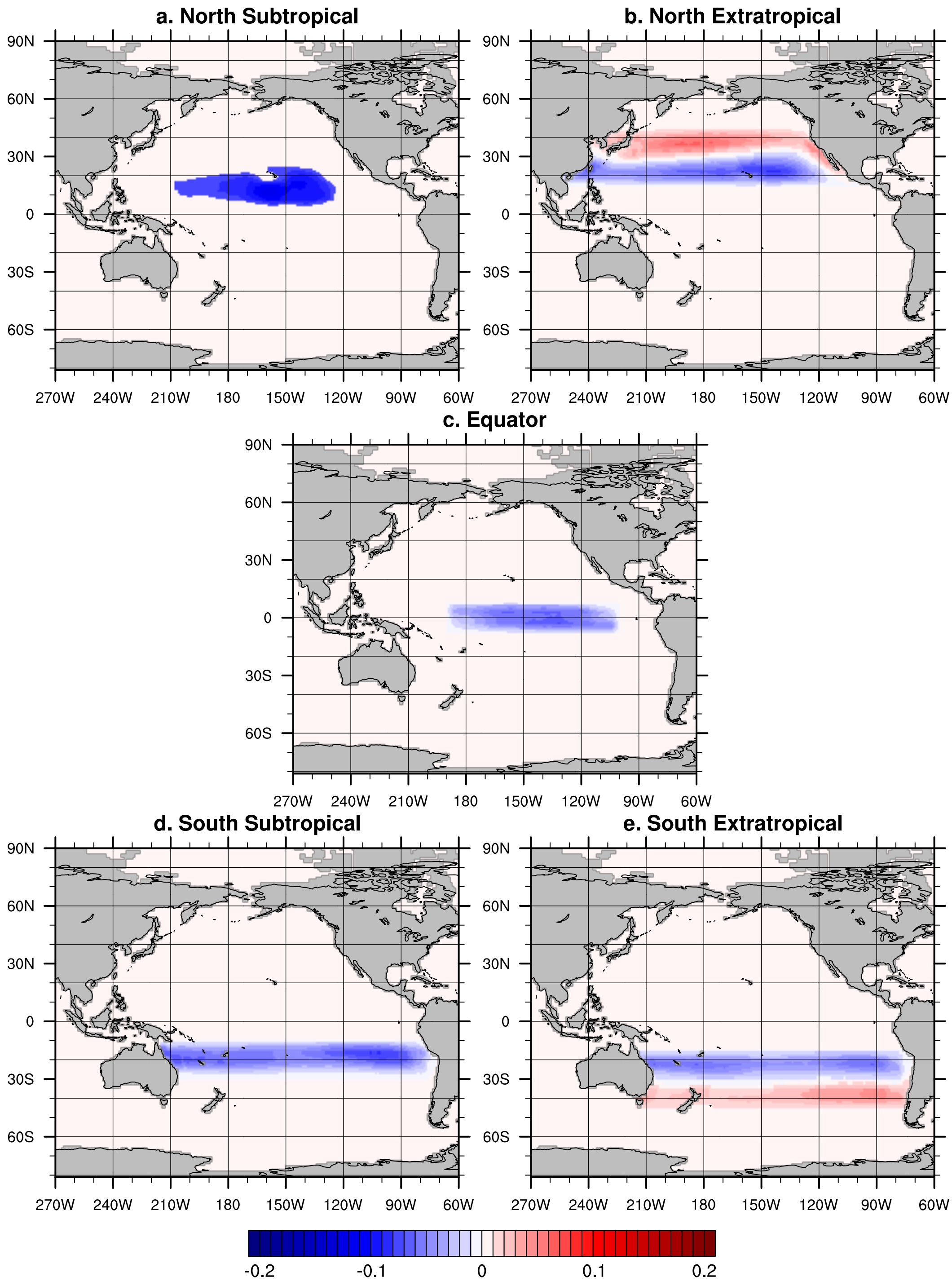

649 FIG. 2. Zonal wind stress (N/m^2) anomalies and their location. Plotted are the climatological values of the zonal wind stress from the CORE-I dataset (Griffies et al. 2009), which are multiplied by a factor and then added to or subtracted from the applied wind stress field.

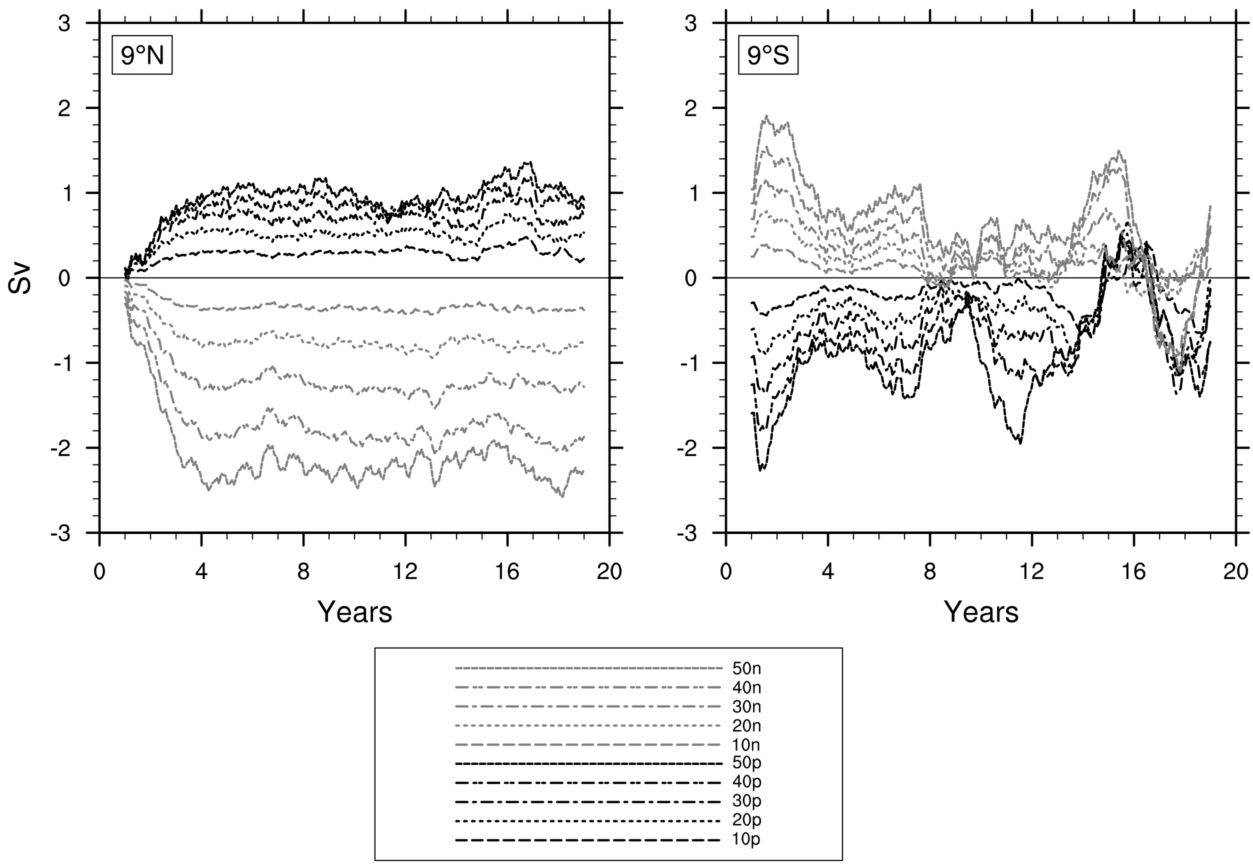

652 FIG. 3. Time series (25-months running mean) of the zonally and vertically-integrated anomalous equatorward
653 transport (Sv) for the equatorial experiments at 9° of each hemisphere in the Indo-Pacific Ocean. Anomalies are
654 computed as deviations from the control value. In the legend, *p* refers to strengthened anomalies and *n* to
655 weakened anomalies.

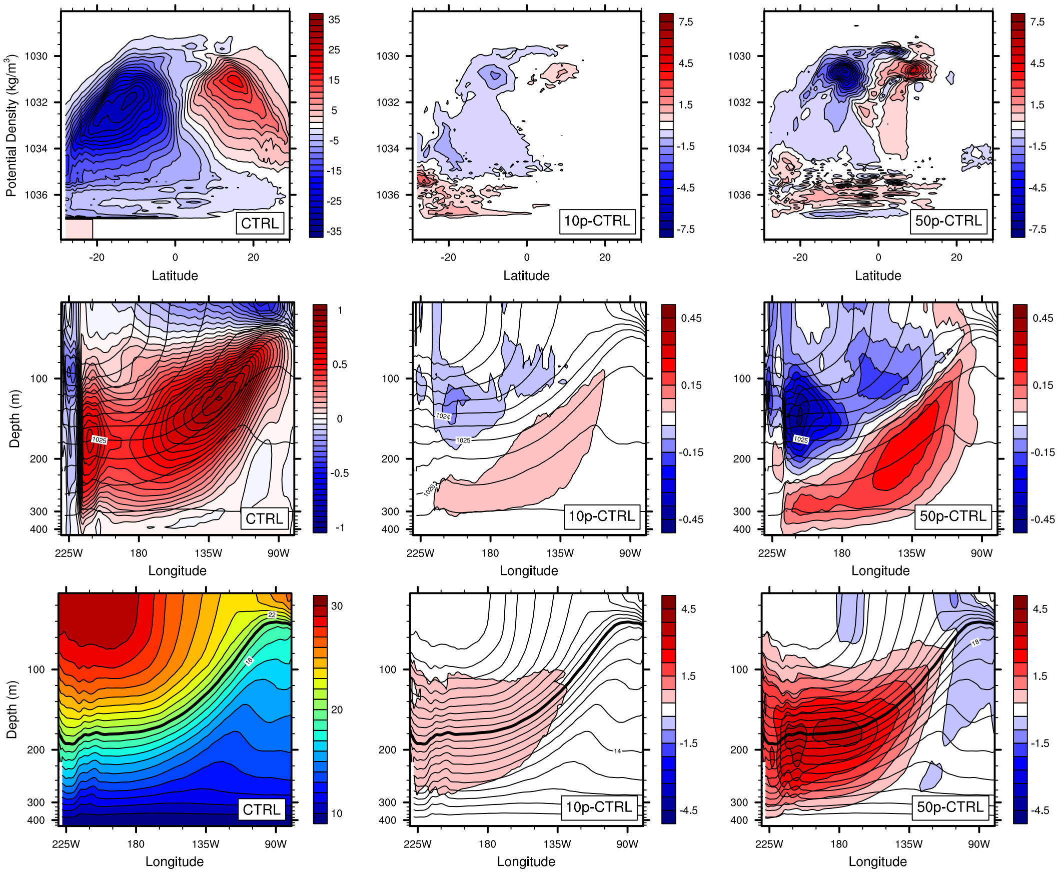

FIG. 4. (Top panels) Zonally-integrated mass transport on density coordinates over the Indo-Pacific Ocean. Time-mean overturning (left), 10% (center) and 50% (right) anomalies for the strengthened equatorial experiments. Red structures are clock-wise cells and blue ones are counterclock-wise. Units are Sverdrup (1 Sv = 10^6 m^3 s^{-1}). (Central panels) Meridional cross sections of zonal velocity (m/s) at the Equator for the control run (left panels, contours), and anomalies for the 10% and 50% (middle and right panels, contours) strengthened equatorial experiments, superimposed on isolines of potential density (kg m^{-3}). (Bottom panels) Meridional cross sections of temperature (°C) at the Equator for the control run (left panels, lines and contours), and anomalies for the 10% and 50% (middle and right panels, contours) strengthened equatorial experiments.

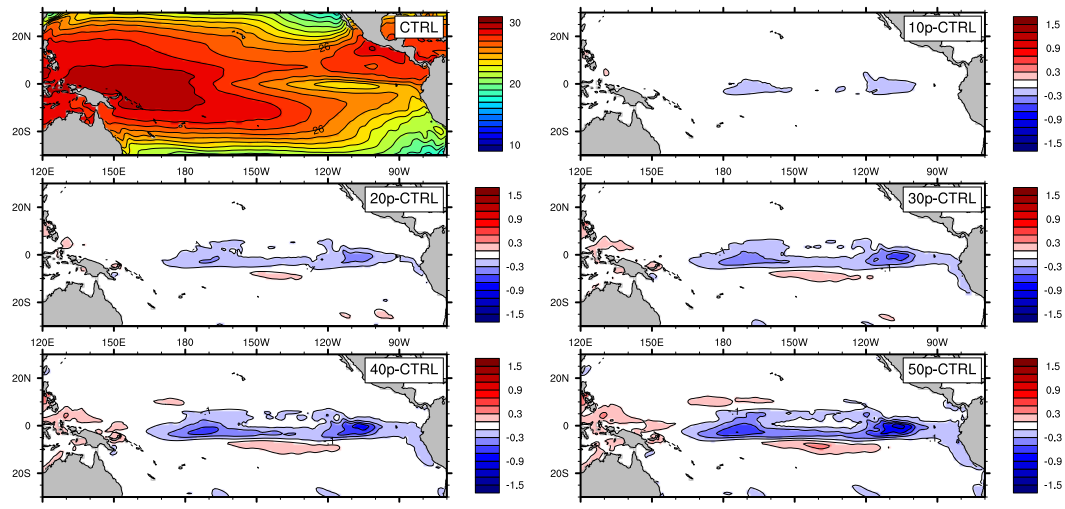

664 FIG. 5. Sea surface temperature (°C) for the control run (top-left panel), and anomalies for the strengthened
665 equatorial experiments.

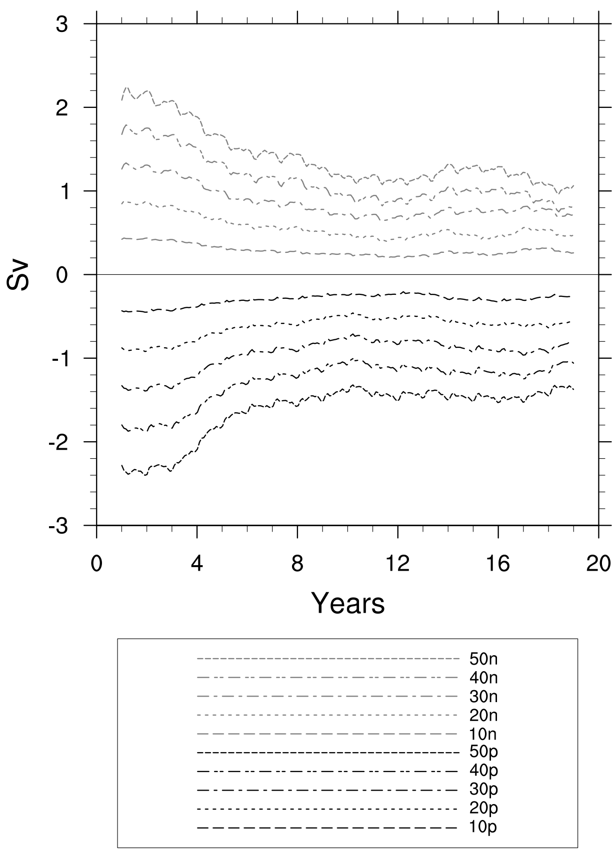

666 FIG. 6. Time series (25-months running mean) of the Indonesian ThroughFlow mass transport (Sv) for the equatorial experiments, shown as anomalies of the control run. In the legend, *p* refers to strengthened anomalies and *n* to weakened anomalies.

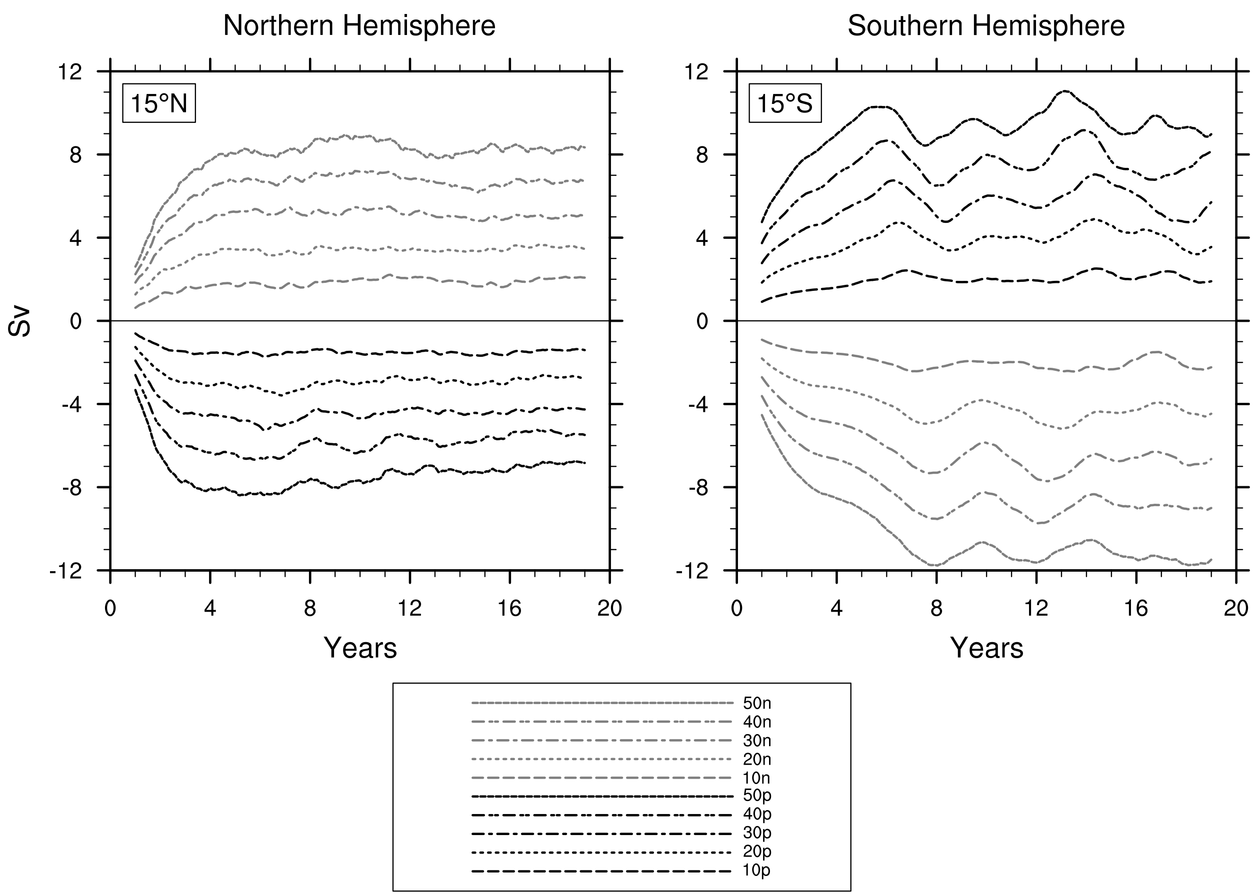

669 FIG. 7. As in Fig. 3 but for the northern subtropical (left panel) and the southern subtropical (right panel)
670 experiments at 15° of each hemisphere in the Indo-Pacific Ocean.

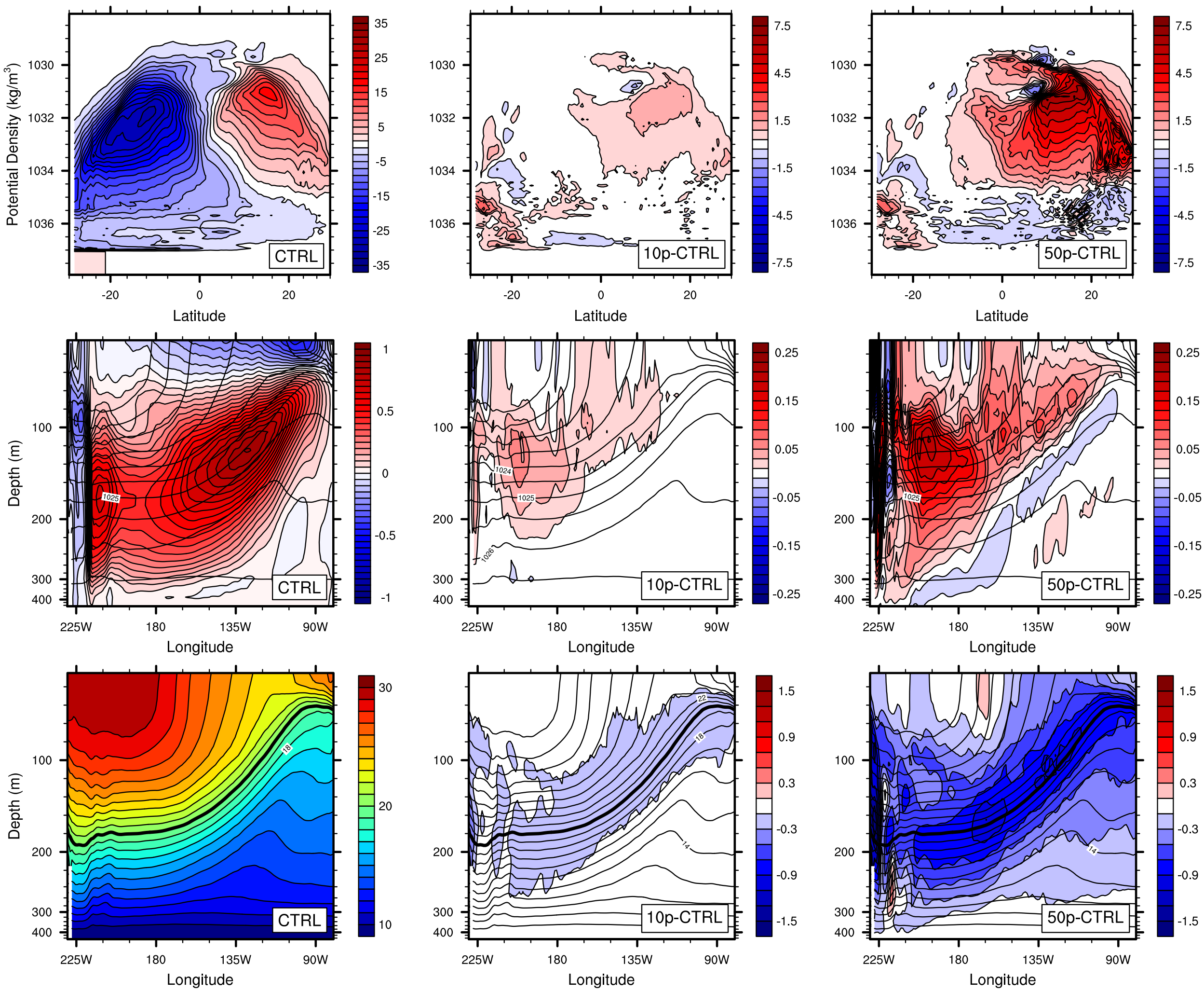

FIG. 8. As in Fig. 4 but for the northern subtropical experiments.

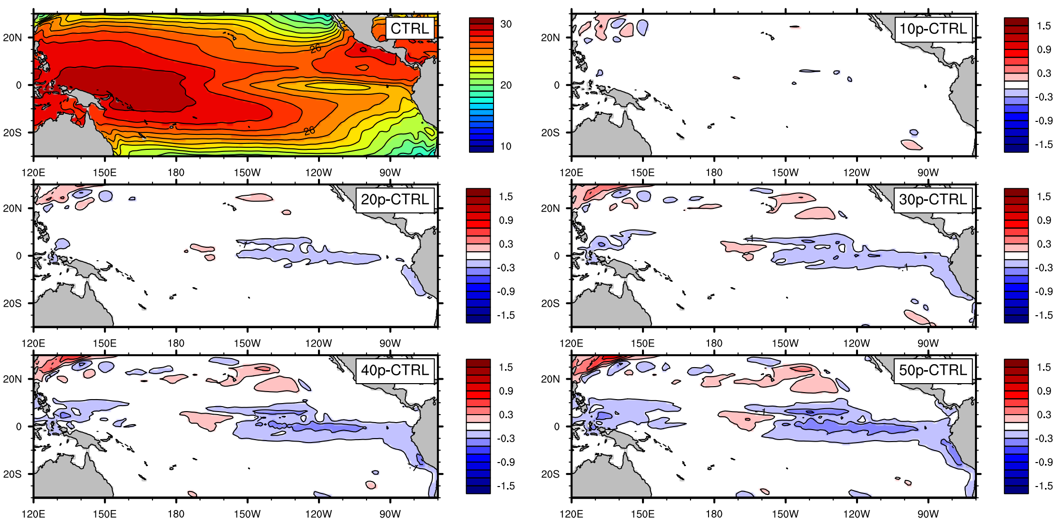

FIG. 9. As in Fig. 5 but for the subtropical experiments.

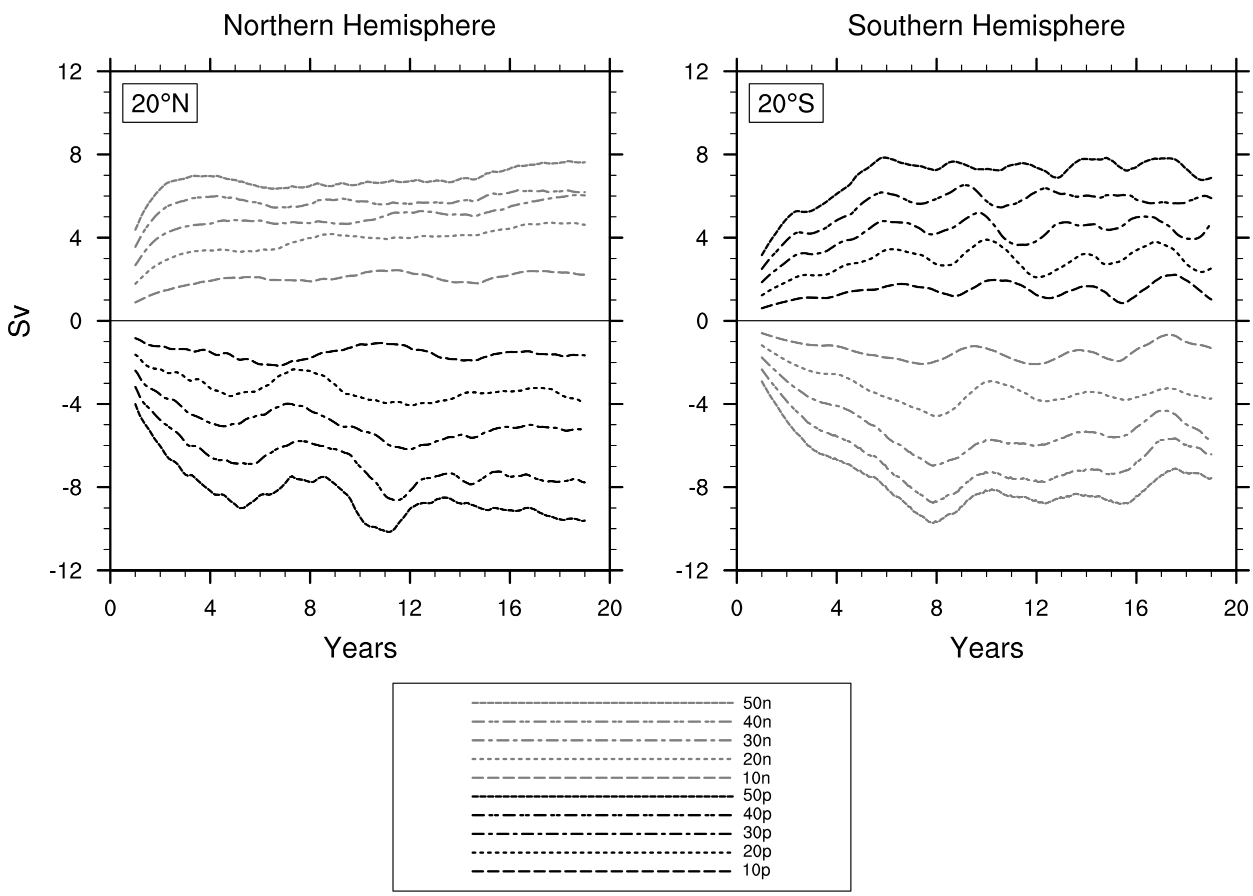

671 FIG. 10. As in Fig. 3 but for the northern extratropical (left panel) and the southern extratropical (right panel) experiments at 20° of each hemisphere in the Indo-Pacific Ocean.

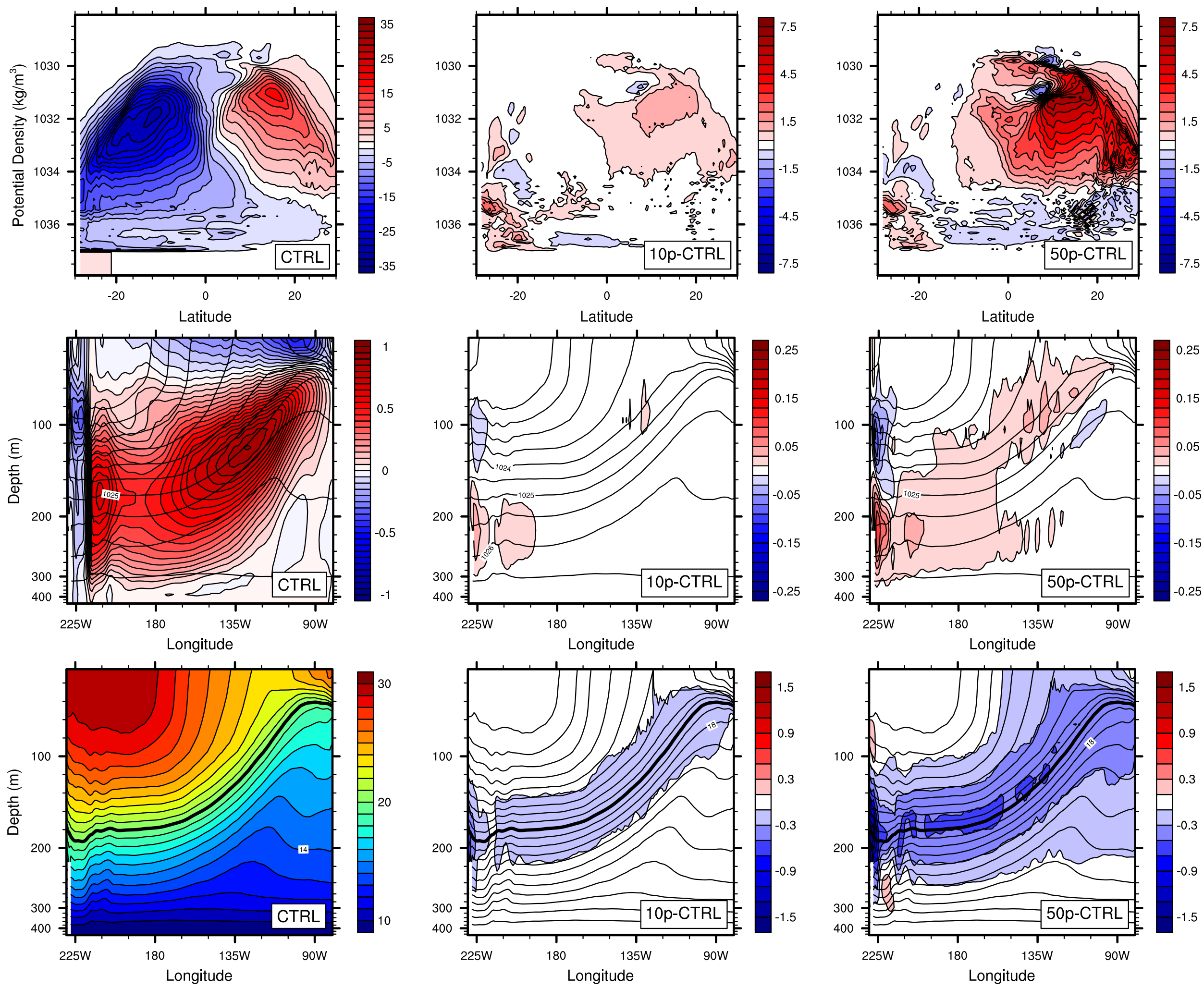

FIG. 11. As in Fig. 4 but for the extratropical experiments.

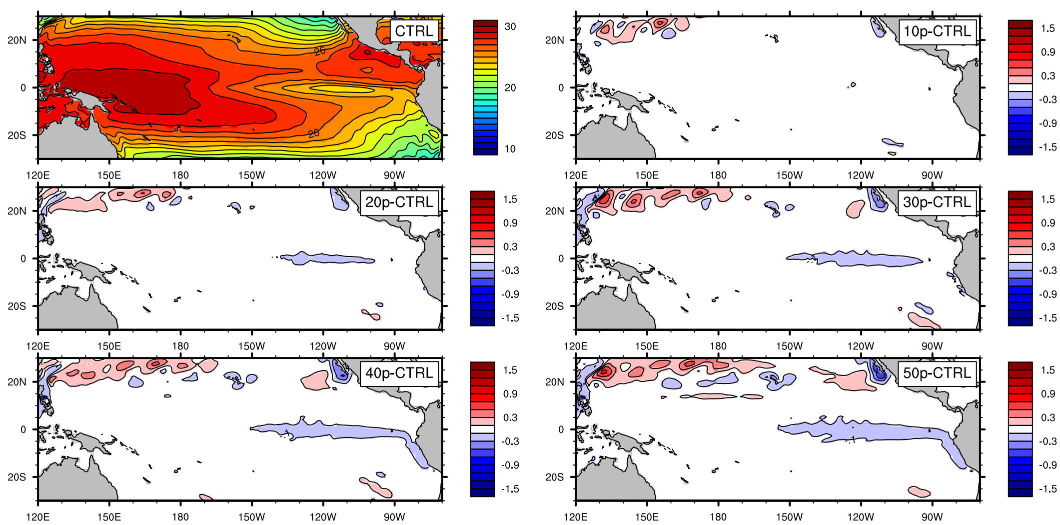

FIG. 12. As in Fig. 5 but for the extratropical experiments.

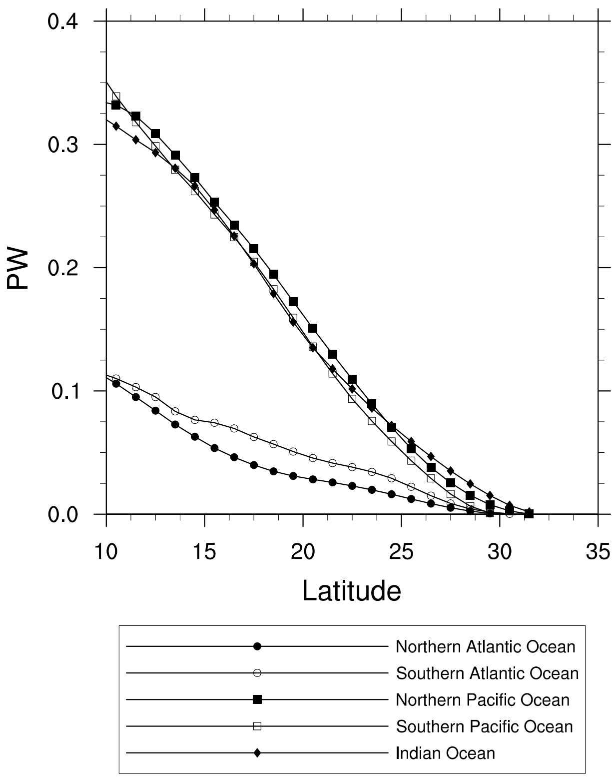

673 FIG. 13. STC meridional energy transports in the control run computed for all basins (1 PW = 10^{15} W).
674 Transports are estimated using Eq. 4 and are in agreement with the observational estimates given in (Klinger
675 and Marotzke 2000, c.f. Fig. 6).

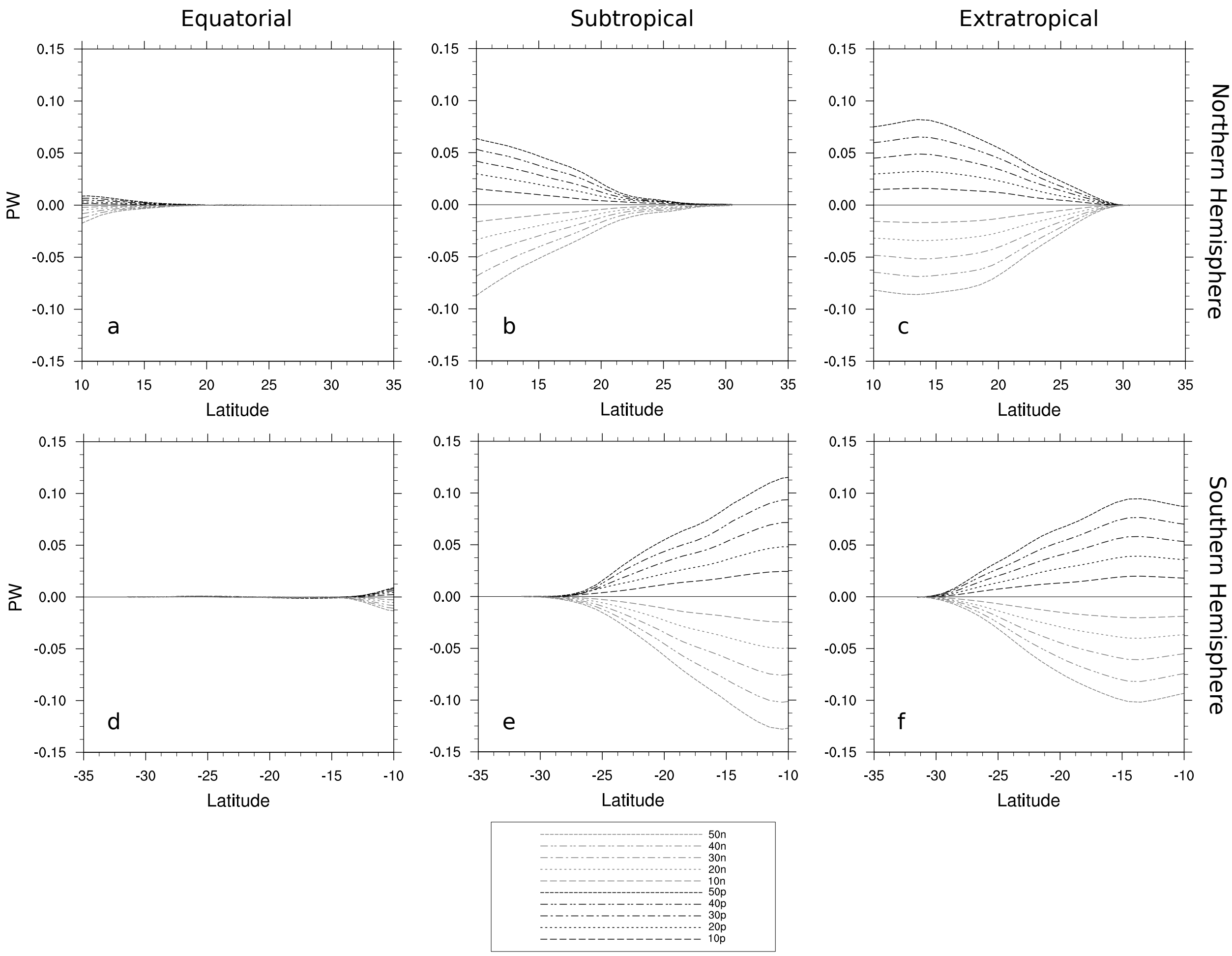

FIG. 14. STC meridional energy transport (1 PW = 10^{15} W) for all northern (top row) and southern (bottom row) experiments, estimated using Eq. 4. Anomalies shown are for the equatorial (left column), subtropical (middle column), and extratropical (right column) experiments. In the legend, *p* refers to strengthened anomalies and *n* to weakened anomalies.

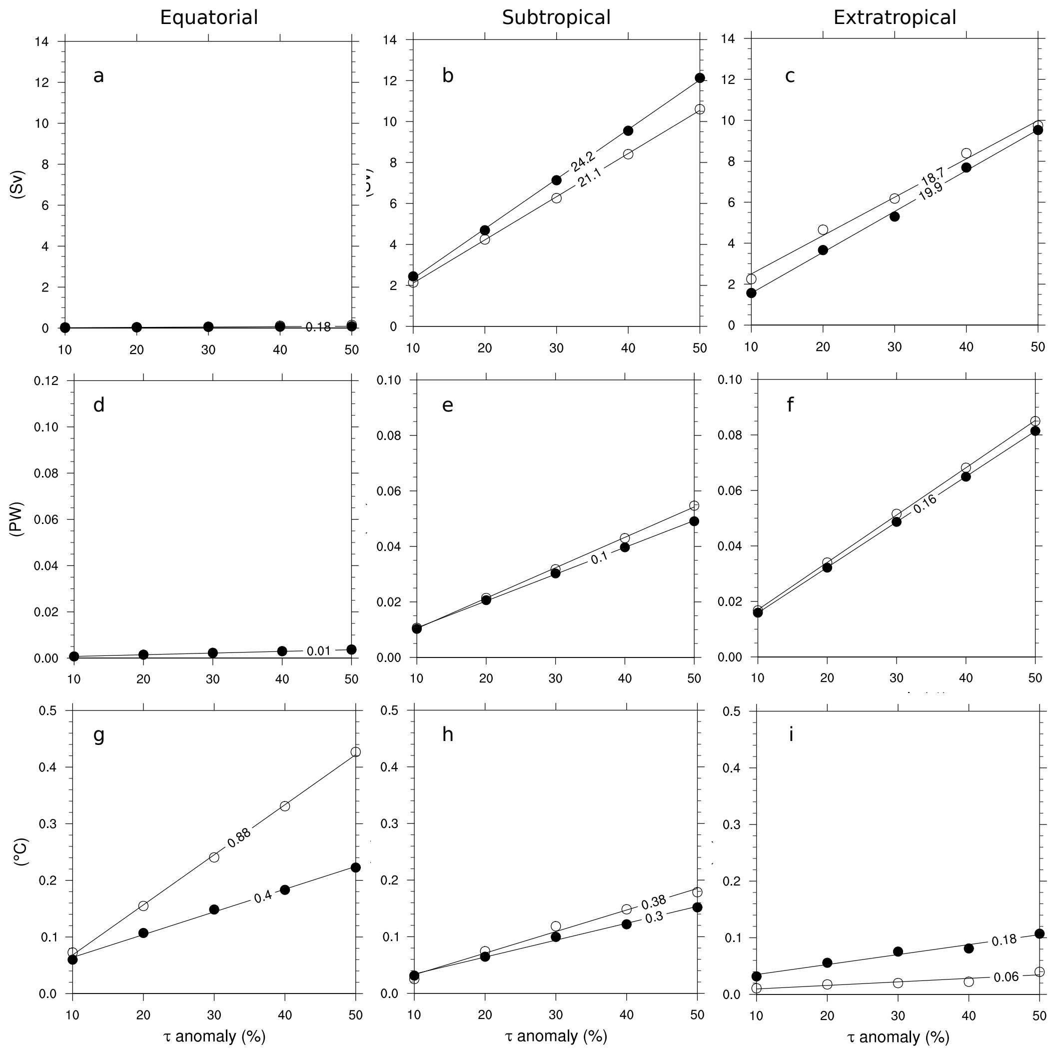

FIG. 15. Wind stress anomaly plotted against the absolute value of anomalies in equatorward mass transport (top row), STC meridional energy transport (middle row) and equatorial SST (right row) for equatorial (left column), subtropical (middle column) and extratropical (right column) wind stress patterns. Mass transports are evaluated as the maximum time-averaged, zonally-integrated, vertically-integrated equatorward mass transport anomaly in the region 10°- 30°N. STC energy transport are evaluated as the time-averaged, zonally-integrated energy tranport anomaly at 15°N. Equatorial SST anomalies are evaluated in the Niño 3.4 region (5°N - 5°S, 120°- 170°W). Solid and empty circles denote strengthened and weakened experiments, respectively. Linear fits are shown for each experimental set, together with the angular coefficient a of the regression line $y = ax$.